

Seasonal variation of CH₄ emissions from central California

Seongeun Jeong,¹ Chuanfeng Zhao,^{1,2} Arlyn E. Andrews,³ Laura Bianco,^{3,4}
James M. Wilczak,³ and Marc L. Fischer¹

Received 23 September 2011; revised 24 February 2012; accepted 30 April 2012; published 12 June 2012.

[1] We estimate seasonal variations in methane (CH₄) emissions from central California from December 2007 through November 2008 by comparing CH₄ mixing ratios measured at a tall tower with transport model predictions based on a global 1° a priori CH₄ emissions map (EDGAR32) and a 10 km seasonally varying California-specific map, calibrated to statewide by CH₄ emission totals. Atmospheric particle trajectories and surface footprints are computed using the Weather Research and Forecasting and Stochastic Time-Inverted Lagrangian Transport models. Uncertainties due to wind velocity and boundary layer mixing depth are evaluated using measurements from radar wind profilers. CH₄ signals calculated using the EDGAR32 emission model are larger than those based on the California-specific model and in better agreement with measurements. However, Bayesian inverse analyses using the California-specific and EDGAR32 maps yield comparable annually averaged posterior CH₄ emissions totaling 1.55 ± 0.24 times and 1.84 ± 0.27 times larger than the California-specific prior emissions, respectively, for a region of central California within approximately 150 km of the tower. If these results are applicable across California, state total CH₄ emissions would account for approximately 9% of state total greenhouse gas emissions. Spatial resolution of emissions within the region near the tower reveal seasonality expected from several biogenic sources, but correlations in the posterior errors on emissions from both prior models indicate that the tower footprints do not resolve spatial structure of emissions. This suggests that including additional towers in a measurement network will improve the regional specificity of the posterior estimates.

Citation: Jeong, S., C. Zhao, A. E. Andrews, L. Bianco, J. M. Wilczak, and M. L. Fischer (2012), Seasonal variation of CH₄ emissions from central California, *J. Geophys. Res.*, *117*, D11306, doi:10.1029/2011JD016896.

1. Introduction

[2] Methane (CH₄) is an important greenhouse gas (GHG), playing a significant role in the climate system, with a global warming potential (GWP) relative to CO₂ estimated at 21 (g CO₂eq/g CH₄) over a 100 year period [Intergovernmental Panel on Climate Change, 1995]. Earth's CH₄ has increased by about 150% since 1750 in concentration, and accounts for ~25% of the total radiative forcing from all long-lived and globally mixed GHGs [Hofmann *et al.*, 2006; Montzka *et al.*, 2011]. Correspondingly,

attention has focused on inverse model assessment of global [e.g., Gimson and Uliasz, 2003; Houweling *et al.*, 1999; Miller *et al.*, 2008], and regional [e.g., Kort *et al.*, 2008; Zhao *et al.*, 2009] CH₄ sources.

[3] At the regional scale, California currently emits approximately 500 Tg of CO₂ equivalent GHGs, with CH₄ currently estimated to contribute approximately 6% of the annual total (California Air Resources Board (ARB), California greenhouse gas emission inventory, 2010, <http://www.arb.ca.gov/cc/inventory/inventory.htm>). Because California has committed to an ambitious plan to reduce emissions to 1990 levels by 2020 through Assembly Bill 32 (AB-32), verifying the success of control strategies will require accounting for CH₄ emissions.

[4] Emission inventories and ecosystem models provide valuable estimates of the spatiotemporal distributions of CH₄ emissions from a variety of sources [Christensen *et al.*, 1996; Potter, 1997; Huang *et al.*, 1998; Matthews *et al.*, 2000; Zhang *et al.*, 2002; Tian *et al.*, 2010; California ARB, online report, 2010]. However, it is difficult to evaluate the inventory model performance at regional scales, largely due to the lack of continuous measurements covering large areas over long periods. Long-term measurements are important because of the strong seasonal dependences of

¹Environmental Energy Technologies Division, Lawrence Berkeley National Laboratory, Berkeley, California, USA.

²Atmospheric, Earth, and Energy Division, Lawrence Livermore National Laboratory, Livermore, California, USA.

³Earth System Research Laboratory, NOAA, Boulder, Colorado, USA.

⁴Cooperative Institute for Research in Environmental Sciences, University of Colorado Boulder, Boulder, Colorado, USA.

Corresponding author: S. Jeong, Environmental Energy Technologies Division, Lawrence Berkeley National Laboratory, MS 90K-127, 1 Cyclotron Rd., Berkeley, CA 94720, USA. (sjeong@lbl.gov)

This paper is not subject to U.S. copyright.
Published in 2012 by the American Geophysical Union.

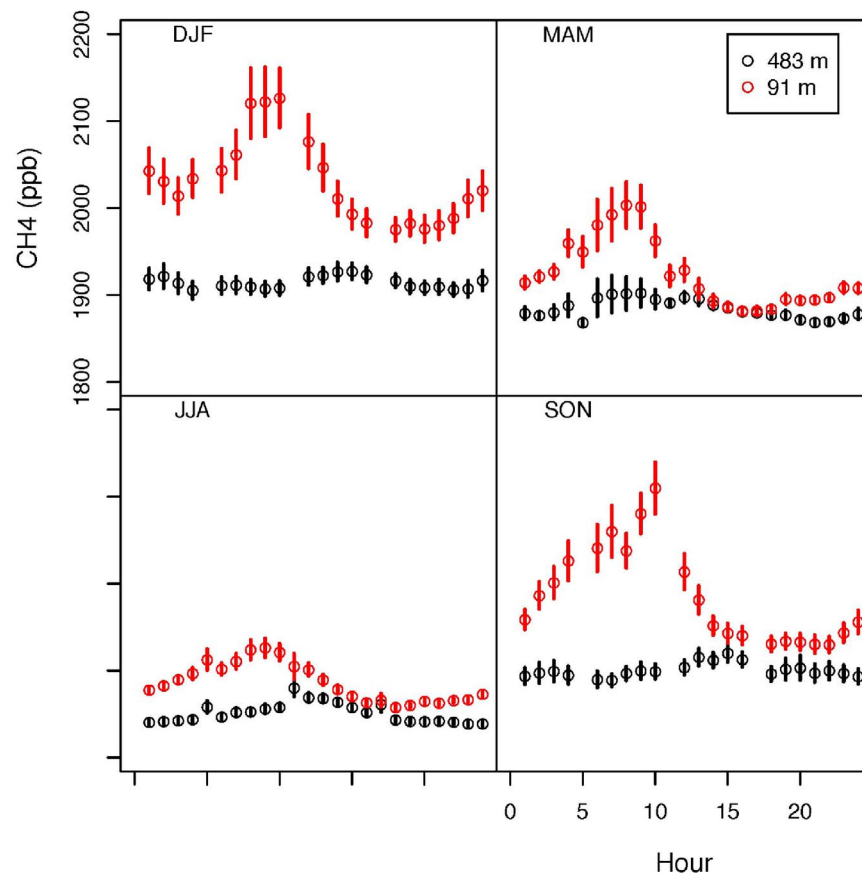


Figure 1. Diurnal cycles of mean hourly (PST) measured CH₄ mixing ratio obtained for 91 and 483 m sampling heights on the WGC tower for the period from December 2007 to November 2008.

CH₄ emissions from natural wetlands [Cicerone *et al.*, 1983; Wilson *et al.*, 1989; Cao *et al.*, 1998], agriculture [Salas *et al.*, 2006; McMillan *et al.*, 2007], and other likely sources. Aircraft measurements provide valuable data for estimating surface CH₄ emissions over short time periods but the high flight expense generally limits long-term monitoring [Matsueda and Inoue, 1999; Wratt *et al.*, 2001; Levin *et al.*, 2002; Gimson and Uliasz, 2003; Kort *et al.*, 2008]. Flux towers provide long-term direct measurements of surface CH₄ emissions, but only over approximately kilometer-scale areas [Mosier *et al.*, 1991; Hansen *et al.*, 1993; Ball *et al.*, 1999; Alm *et al.*, 1999]. Mixing ratio measurements from either towers or space-borne remote sensing can provide continuous long-term measurements, representing larger spatial scales but require inverse techniques to infer emissions [Simpson *et al.*, 1997; Hein *et al.*, 1997; Houweling *et al.*, 1999; Werner *et al.*, 2003; Manning *et al.*, 2003; Bergamaschi *et al.*, 2005; Zhao *et al.*, 2009; Popa *et al.*, 2010].

[5] To date, the seasonal variation in CH₄ emissions from different regions of California has not been quantitatively evaluated. This paper quantifies regional CH₄ emissions from central California over the course of a year period, representing one of the first analyses of seasonal variation in CH₄ emissions from this mixed urban and rural area. The work expands on an initial study by Zhao *et al.* [2009] that quantified CH₄ emissions from central California for a 3 month period from October to December 2007. In section 2

we describe the methods we employed, including atmospheric measurements, a priori CH₄ emissions inventories, mesoscale meteorology and trajectory transport modeling, and the Bayesian inverse method, focusing on the modifications from Zhao *et al.* [2009]. Section 3 describes results, including the seasonal variations in calculated footprints, and the inferred surface emissions of CH₄ from central California for different regions based on simple correlation analysis and the Bayesian analysis of regional emissions. Section 4 summarizes the results and discusses the implications for CH₄ inverse modeling at the regional scale, highlighting the importance of uncertainty in the spatial distribution of a priori emissions and the value of multiple measurement stations.

2. Data and Models

[6] Following Zhao *et al.* [2009], the Bayesian inversion technique employed in this paper obtains posterior CH₄ emission estimates by scaling spatially distributed a priori emissions to minimize the difference between tower-based CH₄ mixing ratios and model predictions. Correspondingly, the data sets used in the inversion technique include tower measurements of CH₄ mixing ratios, a priori CH₄ emission maps, trajectories used for CH₄ predictions, modeled meteorology used to drive the transport model and the estimated boundary condition at the edge of the modeling domain.

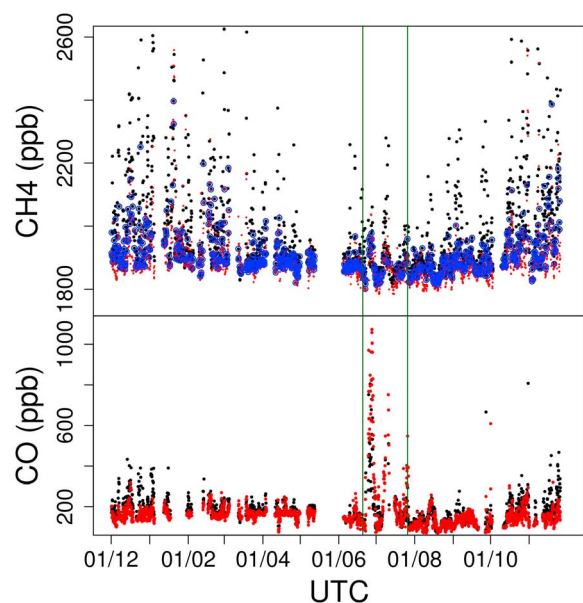


Figure 2. Tower measurements of (top) CH₄ and (bottom) CO at 91 m (black) and 483 m (red) as functions of date (expressed as day/month) for the period between December 2007 and November 2008. The blue circles indicate the data satisfying the well-mixed criteria in this study. The vertical bars indicate the fire period from 20 June to 28 July 2008, which was excluded from further analysis.

2.1. Measurements

[7] CH₄ measurements were made at 91 and 483 m above ground level on a tall tower near Walnut Grove, California (WGC, 121.49°W, 38.27°N, 0 m above sea level), beginning in September 2007. The CH₄ mixing ratios at each height are measured every 15 min and averaged into the 3 h means used in this study. Detailed information about the instrument design is described by Zhao *et al.* [2009] and will not be repeated here. The measurement accuracy, determined by comparison with time synchronized flask sampling and laboratory analysis at NOAA, is ~ 1 ppbv CH₄ during periods when variations in the continuous CH₄ measurements are small enough to allow clear comparison with the relatively rapid (~ 1 min) flask sampling. This accuracy is both significantly smaller than the measured variations in CH₄ at the tower site and likely insignificant compared to the uncertainties in model predictions of CH₄ mixing ratio described below.

[8] A subset of the measured data was selected for the inverse analysis based upon a “well-mixed” requirement limiting the vertical gradient in CH₄ mixing ratio. As shown in Figure 1, the seasonal mean diurnal cycles of CH₄ mixing ratio for air sampled from the 91 and 483 m levels are typically most similar from afternoon to late evening, with differences of ~ 50 ppb in winter and ~ 10 ppb in summer. Data were then selected such that the CH₄ mixing ratio difference between 91 and 483 m fell within the range $-1 \text{ sd} < (C_{91} - C_{483}) < 3 \text{ sd}$, where sd is the standard deviation of the difference of the mean cycle between beginning of afternoon and late evening (1200 and 2300 local time). Based on this criteria, between 60 and 90% of the data from the afternoon

to late evening time window were retained for the inverse analysis in summer and winter, respectively. For example, the December 2007 to November 2008 data are shown in Figure 2 (top), in which the blue circles indicate the data satisfying well-mixed criteria in this study.

[9] In addition to requiring well-mixed conditions, the data were screened to remove periods with obvious contamination from wild fires that were not included in our emission maps (e.g., forest fires). The summer of 2008 included a period with significant fire activity based on the report from the California Department of Forestry and Fire Protection (CDFFP) [Office of Emergency Services, 2008]. To identify the summer 2008 period with potential CH₄ sources due to the fires (that are not present in our inventory), we used CO measurements from an instrument similar to that described in Potosnak *et al.* [1999] in the NOAA tall tower network (<http://www.esrl.noaa.gov/gmd/ccgg/towers/>). Based on the CO measurements for the period from December 2007 to November 2008, which are shown in Figure 2 (bottom), we identified and excluded the significant fire events that affected Northern and central California from 20 June to 28 July 2008. Because the CO screening is not perfect, we note that lower levels of CH₄ emissions from agricultural and heating related biomass combustion could be present in our posterior emission estimates.

[10] We estimate uncertainties in modeled atmospheric transport using measured planetary boundary layer (PBL) heights retrieved from radar wind profilers located near Sacramento (SAC; 121.42°W, 38.30°N), Chowchilla (CCL; 120.24°W, 37.11°N), Chico (CCO; 121.91°W, 39.70°N), and Livermore (LVR; 121.90°W, 37.71°N). Boundary layer depths were estimated using methods described previously [Bianco and Wilczak, 2002; Bianco *et al.*, 2008; Bianco *et al.*, 2011] which can estimate daytime PBL heights from about 150 m to 4000 m with an RMS error of ± 200 m [Dye *et al.*, 1995].

2.2. Prior CH₄ Emission Map

[11] WGC is located in a region containing natural gas fields and wetlands to the West, rice agriculture and natural gas fields to the North, livestock agriculture to the South, and landfills in the regional landscape. To account for this complexity in the landscape of central California, we have improved mapping of the spatial distribution of CH₄ emissions. The new maps update the emission maps from Zhao *et al.* [2009] to more accurately capture the spatial information available to map CH₄ emissions, scaled to the 2008 statewide sums contained in the California ARB CH₄ emission inventory by emissions sector (California ARB, online report, 2010). Relevant to the following work, readers should note that the subregion classification for emission estimates described in Zhao *et al.* [2009] is shown in Figure 3a. In this section, major improvements for a priori emissions over Zhao *et al.* [2009] are described. First, the spatial distribution of CH₄ emissions from dairy livestock (LS) are improved by using a map of dairy livestock density supplied by the California Department of Water Resources scaled to annual CH₄ emissions assuming a constant emission factor of 0.39 kg C/cow/d from the recent work of Salas *et al.* [2009], resulting in total CH₄ emissions from livestock that are 1.8 times the total livestock emission estimate from Zhao *et al.* [2009] (Figure 3b).

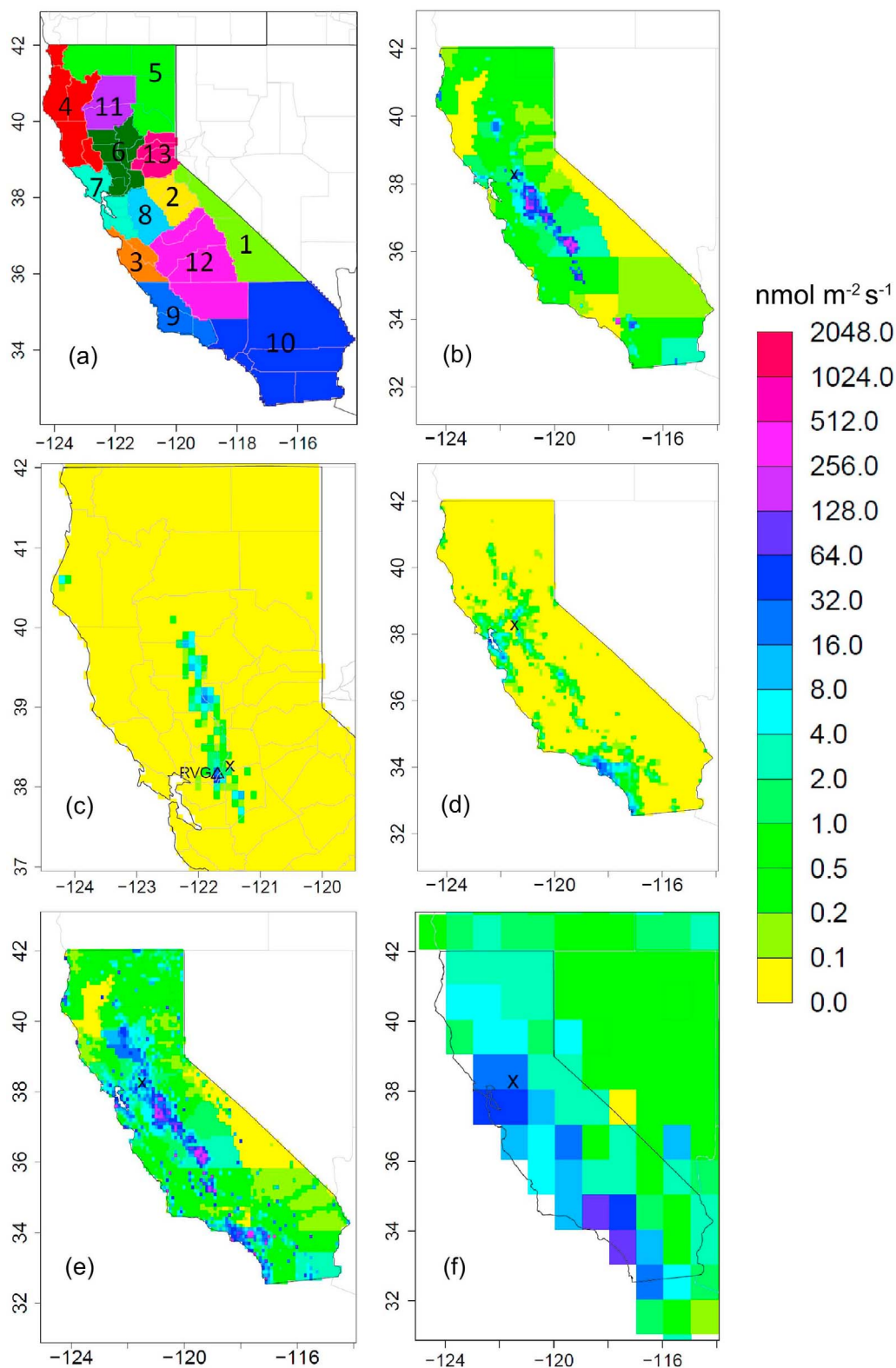


Figure 3. Maps showing (a) region classifications as well as a priori CH₄ emissions from (b) livestock, (c) natural gas wells, (d) natural gas based on California population density, (e) the total California-specific emission model, and (f) the EDGAR32 emission model. The location of the tower is marked with a cross near longitude 121°W, latitude 38°N. The triangle in Figure 3c represents the location of the Rio Vista Gas (RVG), which is one of the largest gas fields in California.

Table 1. A Priori Emissions from the California-Specific and EDGAR32 Models for the Three Regions Near the WGC Tower^a

Regions	California-Specific Seasonal				California-Specific Annual	EDGAR32
	Winter	Spring	Summer	Fall		
R06	1.35	1.70	5.13	2.59	2.69	3.59
R07	1.27	1.27	1.30	1.29	1.28	8.21
R08	5.02	5.01	5.33	5.25	5.15	3.10
Total	7.64	7.98	11.76	9.13	9.13	14.90

^aA priori emissions, Tg CO₂eq yr⁻¹ assuming a global warming potential of 21 g CO₂eq/g CH₄.

[12] Second, we identified natural gas wells in California using information from California Department of Conservation (CDC, <http://www.consrv.ca.gov/dog/Pages/statistics.aspx>) to generate a new emission map from gas wells, which were not accounted for in Zhao *et al.* [2009]. CH₄ emissions from gas wells are estimated using gas production information from California Department of Conservation [2009]. Harrison *et al.* [1997] estimated CH₄ emissions equivalent to $1.4 \pm 0.5\%$ of gross natural gas production for the 1992 baseline year for the entire gas production processes from field production to distribution. Since the available data for this study do not provide detailed information of gas production processes for individual gas fields or wells, we assumed a leakage rate of 1% related to gas production and transmission/storage processes in the gas fields. CDC Districts 5 and 6 are within the footprint region of WGC. However, the gas production of District 5 is only 5% of that of District 6. Thus, we focus on natural gas emissions from District 6 where most wells produce natural gas only, and total gas production (for 2008) was 2.31×10^9 m³. Figure 3c shows the resulting CH₄ emission map from natural gas wells. The remaining Districts (1–4) in the southern San Joaquin Valley and other locations in Southern California are primarily operated to produce liquid petroleum, but also produce a significant amount of “associated” natural gas. Because the fractional CH₄ leakage rate from the petroleum facilities are likely different from that for the natural gas fields and because the WGC footprints have weak sensitivity to Districts 1–4, CH₄ emissions from Districts 1–4 are estimated from California mandatory reports on oil and gas. The remainder of natural gas emissions was apportioned by population density in California using 4 km population maps available from the Socioeconomic Data and Applications Center (Center for International Earth Science Information Network (CIESIN) and Centro Internacional de Agricultura Tropical (CIAT), Gridded population of the world, version 3, population density grid, 2005, <http://sedac.ciesin.columbia.edu/gpw>) so that the statewide total estimate from natural gas matched the California ARB inventory. Total natural gas emissions based on California population density are shown in Figure 3d.

[13] Third, we used seasonally varying CH₄ emissions for agricultural CH₄ sources. Monthly averaged CH₄ emission maps for county level agricultural CH₄ fluxes were taken from the denitrification and decomposition model (DNDC) output (assuming the 1983, high irrigation case) described by Salas *et al.* [2006]. Wetland CH₄ emissions were taken from monthly averages of the Carnegie-Ames-Stanford Approach CH₄ (CASA-CH₄) model from Potter *et al.* [2006]. The resulting maps capture the strong seasonality in these emission sources near the WGC tower. Rice

agriculture is concentrated in Region 6 while other regions have negligible emissions from it. Rice agriculture accounts for 46% of the total CH₄ emissions in Region 6 in annual average, with estimated emissions of 0.33, 3.63, 1.08 and 0 Tg CO₂eq yr⁻¹ for spring, summer, fall and winter, respectively. Similarly, wetland emissions also show a seasonal variation with summer having the maximum, but represent only 6.7, 2.5, 5.2% of the total CH₄ emissions for Regions 6, 7 and 8, respectively.

[14] Figure 3e shows total California-specific CH₄ surface emissions with a high resolution (~10 km), and the EDGAR 32FT2000 (EDGAR32 hereafter) CH₄ emission map (~100 km) [Olivier *et al.*, 2005] is shown in Figure 3f. Seasonal CH₄ emissions for the three regions (6, 7 and 8) near the WGC tower are summarized and compared with the EDGAR32 emissions in Table 1. It is worth noting that the EDGAR32 maps especially give large weight to the San Francisco Bay urban area (Region 7), while the California-specific map gives more weight to the Central Valley (Regions 6 and 8).

2.3. Trajectory and Meteorology

[15] Predicted contributions to CH₄ mixing ratios from emissions within the modeling domain are calculated as $\mathbf{F}\mathbf{e}$, where \mathbf{F} is footprint strength, and \mathbf{e} is the a priori CH₄ emissions. Footprints are calculated from particle trajectories simulated using the Stochastic Time-Inverted Lagrangian Transport (STILT) model [Lin *et al.*, 2003, 2004]. In this study, 500 particles are released hourly (from UTC hour 00) at the WGC tower (91 m) and transported backward in time 7 days to insure a majority of the particles reach positions representative of the marine boundary layer. The meteorology used to drive this transport model is from the simulation of Weather Research and Forecasting (WRF2.2) model [Skamarock *et al.*, 2005]. WRF2.2 has been slightly modified to be coupled with STILT (WRF-STILT) by Nehr Korn *et al.* [2010].

[16] The WRF model simulations follow those described in Zhao *et al.* [2009] with the following two modifications. First, the PBL scheme was changed from the Yonsei University (YSU) scheme to the Mellor-Yamada-Janjic (MYJ) TKE scheme [Mellor and Yamada, 1982; Janjić, 1990]. Second, we nested subdomains using spatial resolutions of 36, 12, and 4 km (shown in Figure 4) at a ratio of 1/3 (rather than 1/5 used in Zhao *et al.* [2009]) to reduce discontinuities, and employed 50 vertical layers between surface and 100 mb to better resolve the planetary boundary layer. Subdomains were computed with one-way nesting from the next outer subregion. Each day was simulated separately using 30 h run (including 6 h from the previous day for spin-up) with hourly output. And the forecast fields were nudged to the

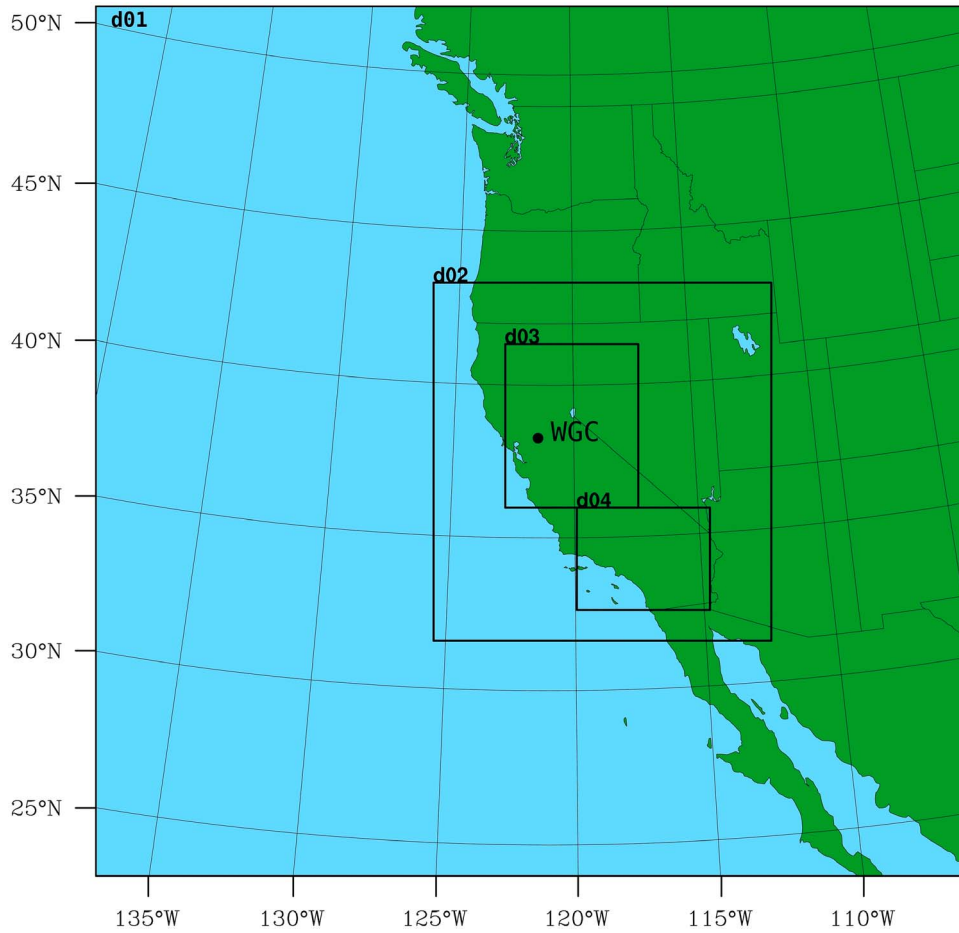


Figure 4. WRF initial boundary set up with three-level nested domains. The ratio of spatial resolution between the three levels is 3. The resolutions for d01, d02, d03, and d04 are 36, 12, 4, and 4 km, respectively.

gridded North American Regional Reanalysis (NARR) [Mesinger *et al.*, 2006] fields (32 km resolution) every 3 h.

2.4. Bayesian Inverse Model

2.4.1. Inversion Approach

[17] We apply a scaling factor Bayesian inversion (SFBI) method to estimate seasonal variations in CH₄ emissions from central California using measured CH₄ mixing ratios at a tall tower. As described in Gerbig *et al.* [2003], Lin *et al.* [2003] and Zhao *et al.* [2009], the local CH₄ mixing ratio at the receptor **c** can be modeled as

$$\mathbf{c} = \mathbf{K}\boldsymbol{\lambda} + \mathbf{v} \quad (1)$$

where $\mathbf{K} = \mathbf{F}\mathbf{e}$, $\boldsymbol{\lambda}$ is a state vector for scaling factors, which is used to adjust emissions from sources or regions, and \mathbf{v} is a vector representing the model-data mismatch with a covariance matrix \mathbf{R} . We model \mathbf{R} as a diagonal matrix to represent the total variance associated with all error sources such as the measurement error and the transport error. Following the Gaussian assumptions, the posterior estimate for $\boldsymbol{\lambda}$ is

$$\boldsymbol{\lambda}_{\text{post}} = (\mathbf{K}^T \mathbf{R}^{-1} \mathbf{K} + \mathbf{Q}_{\lambda}^{-1})^{-1} (\mathbf{K}^T \mathbf{R}^{-1} \mathbf{c} + \mathbf{Q}_{\lambda}^{-1} \boldsymbol{\lambda}_{\text{prior}}) \quad (2)$$

where $\boldsymbol{\lambda}_{\text{prior}}$ is the a priori estimate for $\boldsymbol{\lambda}$, and \mathbf{Q}_{λ} is the error covariance associated with $\boldsymbol{\lambda}_{\text{prior}}$. Uncertainty associated

with total anthropogenic CH₄ emissions in the U.S. ranges from 10% to 50%, and emission uncertainty for rice agriculture is greater than 50% [Committee on Methods for Estimating Greenhouse Gas Emissions, 2010]. Committee on Methods for Estimating Greenhouse Gas Emissions [2010] also reported that emission estimate uncertainties for manure management and fugitive emissions from fuels are highly variable (less than 10%–100%). Because the central California region includes such uncertain CH₄ emission sources as rice agriculture, livestock and natural gas fields, we use 50% uncertainty in our a priori emission models for the baseline analysis. The posterior error covariance for $\boldsymbol{\lambda}$ is given by

$$\mathbf{V}_{\text{post}} = (\mathbf{K}^T \mathbf{R}^{-1} \mathbf{K} + \mathbf{Q}_{\lambda}^{-1})^{-1} \quad (3)$$

To determine optimal emissions, we use the SFBI method at a monthly temporal scale based on the two CH₄ a priori emission models described in section 2.2. In this paper, however, most of the results are summarized seasonally. We combine May with April and July with June because the number of observations for May and July is much smaller than the other months due to missing data and removal of data from wild fire periods. The inverse modeling approach is applied in two phases as in Bergamaschi *et al.* [2005]. A

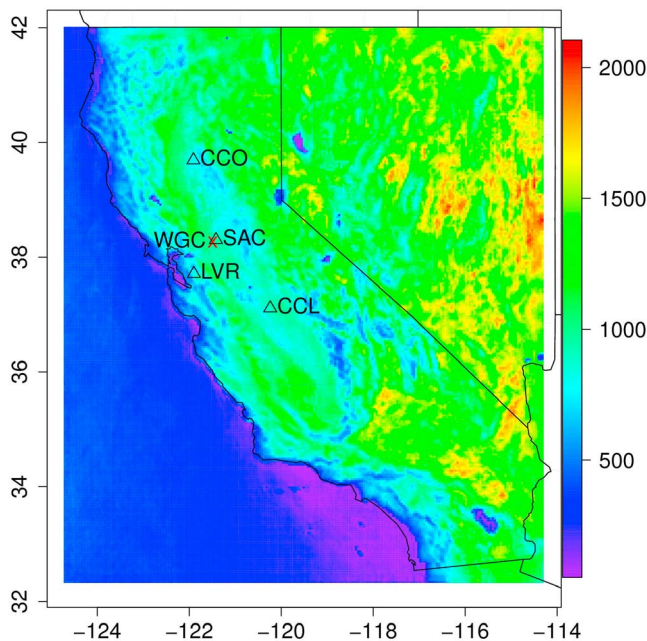


Figure 5. Map of central California showing the location of Walnut Grove Tower (WGC; red cross) and the locations of the four radar wind profilers (black triangles) at Sacramento (SAC), Chico (CCO), Chowchilla (CCL), and Livermore (LVR), with predicted monthly mean PBL heights (m) for June 2008, 10:00 PST, shown in color.

first inversion is conducted based on the data selected using the well-mixed condition criteria described in section 2.1. The second (final) inversion uses data points that are accepted by applying the selection criteria $|c_i - (K\lambda)_i|^2 < \alpha R_i$, where α is a fixed value for each month. As in the first inversion, the final inversion is performed using the original a priori emission maps, and therefore the first inversion is used as a data selection tool for the atmospheric observations. This phased approach removes outliers that might otherwise induce biases in the inversion. Bergamaschi *et al.* [2005] accepted data for $\alpha = 2$, though they found that relaxing α to 3 had a very small effect on the posterior λ . In this study, we choose the value of α for each month via an iterative process such that the chi-square values from the final inversion are close to unity [Tarantola, 1987]. A sensitivity analysis for α is described in section 3.4.

2.4.2. Error Covariance Analysis

[18] Following Gerbig *et al.* [2003], Zhao *et al.* [2009], and Göckede *et al.* [2010], the diagonal elements of the model-data mismatch matrix \mathbf{R} are estimated from the linear sum of contributing uncertainties in the footprints (e.g., number of particles released, flux aggregation at finite resolution, uncertainties in modeled transport winds and PBL), the estimated CH₄ background, and the a priori emissions. Here,

$$\mathbf{R}_i = \mathbf{S}_{\text{part}} + \mathbf{S}_{\text{aggr}} + \mathbf{S}_{\text{bkgd}} + \mathbf{S}_{\text{TransPBL}} + \mathbf{S}_{\text{TransWIND}}, \quad (4)$$

where errors are calculated by comparing the root-mean-square (RMS) differences in simulated CH₄ signals. For the particle number error (\mathbf{S}_{part} , ~5% of background-subtracted

mean signal) the comparison is made between test runs releasing 1000 particles and the bulk runs calculated with the release of 500 particles. The aggregation error (\mathbf{S}_{aggr} , ~11%) is obtained from the comparison made between runs using full (0.1° pixel) fluxes and fluxes aggregated to county level.

[19] For the marine background error (\mathbf{S}_{bkgd}) the comparison is made between the minimum nighttime CH₄ measured at 483 m (presuming near free troposphere values) and values propagated to the tower from a model of Pacific ocean CH₄ mixing ratios. Following Zhao *et al.* [2009], we estimated the background CH₄ mixing ratio using the final latitude of each particle as a lookup into the latitudinally averaged marine boundary layer (MBL) CH₄ (NOAA Globalview CH₄ product, <http://www.esrl.noaa.gov/gmd/ccgg/globalview/index.html>). Only time points for which more than 80% of the particles reached longitudes 1.5° from the coast were included in the study. To account for seasonal variations in background errors, the RMS difference between the MBL background and the 483 CH₄ measurements was calculated for each season. The RMS difference values were 20.3, 14.7, 16.4 and 24.7 ppb for spring, summer, fall, and winter, respectively. These values are significantly higher than the value of 11.7 ppb obtained previously in Zhao *et al.* [2009] although the months and years are different.

[20] As described in Zhao *et al.* [2009], errors due to uncertainties in atmospheric transport are significant. To estimate the uncertainty in predicted CH₄ signals due to errors from modeled PBL heights ($\mathbf{S}_{\text{TransPBL}}$) and winds ($\mathbf{S}_{\text{TransWIND}}$), we evaluated model errors in winds and PBL heights and then calculated the RMS difference in CH₄ signals obtained from simulations with and without input of an additional stochastic component of wind and PBL errors in STILT.

[21] Extending beyond Zhao *et al.* [2009], we evaluated PBL heights (Z_i) at four stations. Figure 5 shows the locations of a nearby (within 8 km of WGC) profiler (SAC), and three more distant profilers near Chowchilla (CCL), Chico (CCO), and Livermore (LVR). Most relevant to the WGC measurements, we compare Z_i from WRF-STILT with measurements from the SAC profiler for January 2008, April 2008, July 2008, and October 2007, the midpoint months of the winter, spring, summer and fall measurement periods. Assuming the uncertainties in modeled and measured Z_i are roughly equal, the geometric linear regressions of modeled on measured Z_i yield regression lines statistically consistent with slopes of 1.00 ± 0.25 , 0.86 ± 0.04 , 1.01 ± 0.08 , and 0.97 ± 0.11 for January, April, July, and October, respectively. The estimated RMS errors were 415 m, 255 m, 159 m, and 289 m for January, April, July, and October, respectively. Assuming the RMS scatter in predicted versus measured Z_i can be represented as the sum of squares of measurement uncertainty (~200 m [Dye *et al.*, 1995]) and WRF-STILT model uncertainty, the RMS error in the WRF-STILT model ranges from very small in summer to near 300 m in winter.

[22] To account for the large seasonal variation in the modeled Z_i , we conducted an error analysis of Z_i for January, April, and July following the method in Zhao *et al.* [2009] while we adopt the error of 24% for October from Zhao *et al.* [2009]. We assumed that the midpoint month of each season represents the total variability of the season.

Table 2. Estimated Model-Data Mismatch Errors and Number of Observations for Final Inversions

	Jan	Feb	Mar	Apr–May ^a	Jun–Jul ^a	Aug	Sep	Oct	Nov	Dec
Model-data mismatch (ppb)	42.0	42.0	21.8	21.8	15.6	15.6	22.0	22.0	22.0	42.0
Number of observations for California-specific model	36	41	60	87	67	53	60	43	44	53
Number of observations for EDGAR32 model	35	42	57	88	68	58	62	42	43	48

^aData for May and July are combined with those of April and June, respectively, due to missing measurements and fire period cuts.

For each season, we perturbed Z_i by 10% and propagated it through transport simulations. Then we computed CH₄ signals (C_{CH_4}) based on the perturbation to estimate their sensitivity to Z_i (i.e., dC_{CH_4}/dZ_i) as a first-order approximation. The dC_{CH_4}/dZ_i values for spring, summer and winter were 0.03, 0.03, and 0.14 ppb m⁻¹, respectively. Due to the large RMS difference between the measured and predicted Z_i , winter showed the largest sensitivity of CH₄ signals to Z_i in conjunction with the high mean seasonal CH₄. By applying the inferred RMS error in the WRF-STILT model to dC_{CH_4}/dZ_i as in *Zhao et al.* [2009], we estimated 6.7, 1.6, 12.3 and 32.0 ppb for errors associated with Z_i for spring, summer, fall and winter, respectively.

[23] Unlike the model-measurement comparison at the SAC site, PBL heights at some other profilers do show small biases. In April 2008, for example, modeled PBL agrees well with the measurements at CCO (slope = 1.03 ± 0.08), but is lower than the measurements at CCL (slope = 0.78 ± 0.06) and LVR (slope = 0.77 ± 0.05). To estimate the effect of these biases, we calculated CH₄ signals for WGC with and without perturbing PBL depths at distant sites and found the errors to be small compared to the measured signals because of the relatively weak footprint strength at distant locations.

[24] Uncertainty in modeled CH₄ signals due to errors in modeled winds is estimated using modeled and measured winds for the 127 m height on the WGC tower in the months of January, April, July, and October. RMS model-data differences in U and V wind velocities range from about 2 to 3 m s⁻¹, without significant biases. The RMS errors for the U component were 2.41, 2.66, 3.03, and 2.88 m s⁻¹ for January, April, July, and October, respectively. For the V component, the RMS errors were 3.11, 2.41, 2.06, and 2.46 m s⁻¹ for the same months. The resulting RMS error in modeled wind was estimated across seasons as 3.7 m s⁻¹. Propagating a random wind component of the velocity error through STILT yielded a typical signal variation of $\sim 10\%$ of the background-subtracted mean CH₄ signal.

[25] Finally, assuming all of the errors from equation (4) are independent, the errors were combined in quadrature to yield a total expected model-data mismatch error and are shown in Table 2 along with the number of observations used in the final inversion. Seasonally estimated model-data mismatch errors are used for all the months belonging to the given season. These errors were used to populate the diagonal elements of **R** in equations (2)–(4). The estimated errors are larger than the estimated error ($\sim 32\%$ of mean CH₄ signal) in *Zhao et al.* [2009], largely due to the estimated uncertainty in PBL depth and background mixing ratios, though the seasons and years are different. This will have the

effect of reducing the influence that the measurements have in perturbing the prior emission models.

3. Results

3.1. Footprints

[26] Figure 6 shows the average footprints during well-mixed periods, for spring (March, April, May), summer (June, July, August), fall (September, October, November), and winter (December, January, February). There is a clear seasonal pattern for the distribution of footprints. In summer, the footprints are strongest from the San Francisco Bay area to the west of the WGC tower (henceforth Bay-WGC) due to the dominance of land-ocean winds; in the transition seasons of spring and fall, footprints are stronger from the North Central Valley due to a shift toward north-south winds; in winter, the footprints are strongest in the Central Valley, while the Bay-WGC region is second in terms of footprint influence.

3.2. CH₄ Mixing Ratios

[27] The CH₄ signals measured at 91 m are compared with WRF-STILT predictions of background CH₄ signals in Figure 7 for well-mixed periods. In general, the variability in measured CH₄ is larger in winter than the other seasons, consistent with a recent analysis of the seasonality of maximum boundary layer depths [*Bianco et al.*, 2011], which showed that the boundary layer height reaches its maximum in late spring months. Similarly, spring months had the lowest value (27.83 ppb) for the background-subtracted mean CH₄ during the well-mixed periods, with summer, fall and winter having 31.29, 51.28 and 72.65 ppb, respectively. In addition, the minimum values reasonably approximate predicted background CH₄ at WGC, showing a smoothly varying seasonality with a maximum centered on winter and a minimum centered on late summer.

3.3. Bayesian Region Analysis

[28] We estimated CH₄ emissions from the different regions in Figure 3a using the SFBI model. As described in section 2.4, the SFBI is first applied to the data selected based on the well-mixed conditions. The first inversion was performed at a monthly scale to avoid temporal aggregation errors, and a total of 628 observations were used to solve for 130 unknowns. After the first optimization, posterior predicted CH₄ mixing ratios from the inversion of California-specific emissions were compared with observations and summarized at the seasonal scale. Results using a chi-square (fitexy) linear regression analysis [*Press et al.*, 1992] yielded fitting slopes (RMS error) of 0.65 ± 0.05 (32 ppb), 0.69 ± 0.14 (26 ppb), 0.79 ± 0.05 (59 ppb), and 0.81 ± 0.05 (66 ppb) for spring, summer, fall, and winter, respectively. The posterior fitting slopes are closer to unity, and the RMS errors are

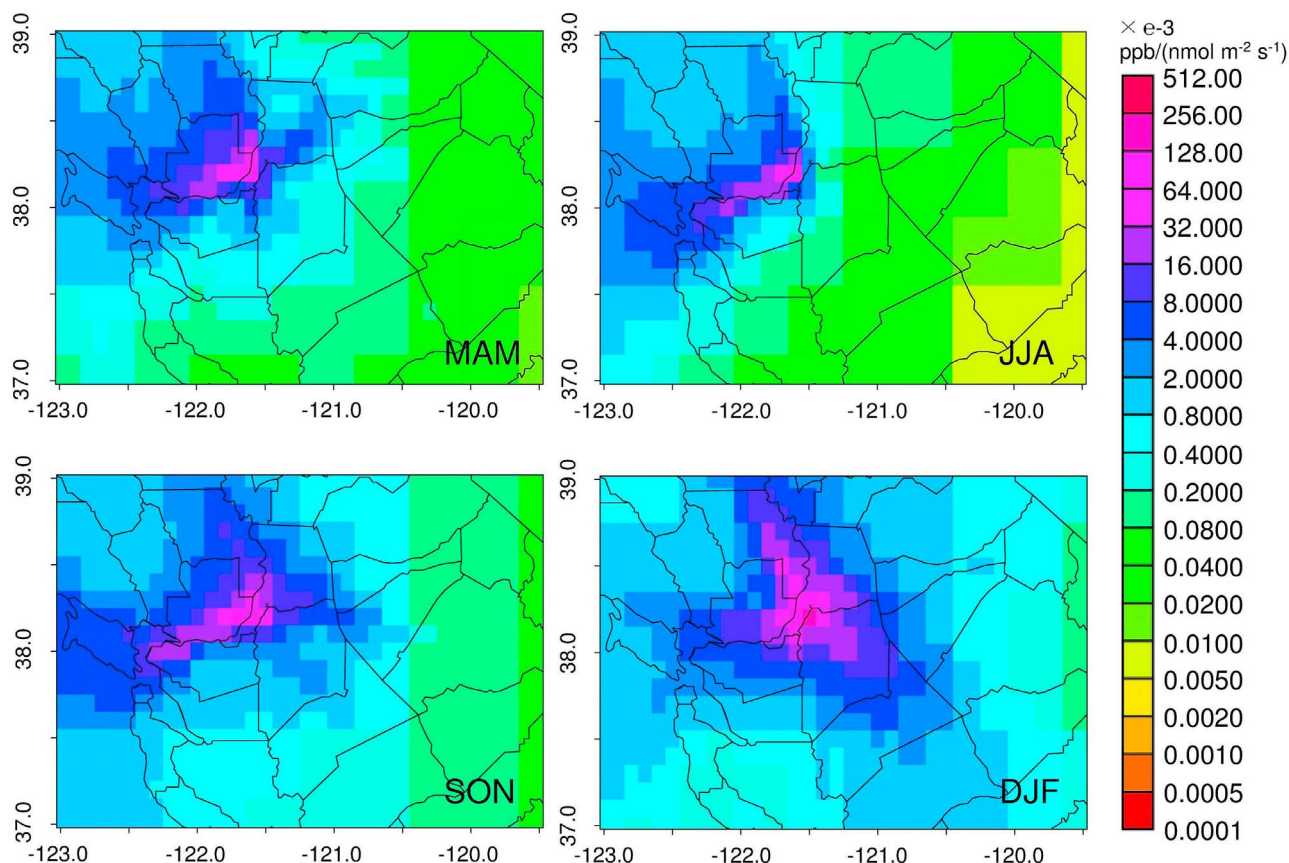


Figure 6. Seasonally averaged footprint maps over well-mixed periods for spring (MAM), summer (JJA), fall (SON), and winter (DJF).

reduced by 19%–22% compared to the results before optimization where RMS errors were 41, 32, 76, and 82 ppb for spring, summer, fall, and winter, respectively and fitting slopes were low (0.3–0.5). This result suggests that the inverse optimization has improved the agreement between the measured and predicted CH₄ signals. However, even after applying the optimized scaling factors, the slopes are still less than unity.

[29] To address the residual underestimation in the predicted CH₄ signals, outlier points are removed based on a requirement that the difference between measured and predicted mixing ratios fall within a factor α (e.g., $\alpha = 2$) of the estimated error [Bergamaschi *et al.*, 2005]. In this study α ranges between 1.9 and 3.2 depending on the month, and sensitivity of emission estimates to α values is discussed in section 3.4.

[30] The outlier removals vary with month, excluding 5–25% (mean removal rate = 13.4%) and 0–27% (mean = 11.8%) of the data used in the first inversion for the California-specific and EDGAR32 models, respectively. For both cases, the fraction of data removed was consistent with the 12–14% removal rate reported by Bergamaschi *et al.* [2005]. We associate the higher fraction of removed data with the overall low emissions in the California-specific model and the differences in spatial distribution of CH₄ emissions between the two a priori models. These outliers may result from uncaptured errors in transport and background signals in our current modeling system. In terms of emission maps, the likely causes of these outliers include

local sources that are not included in the inventory and lack of information on detailed temporal and spatial variations of emissions, in particular near the tower where footprints are strong.

[31] After excluding outliers, the SFBI method is applied as a second inversion, and a total of 544 observations were used to solve for 130 unknowns. Figure 8 shows the regression of posterior predicted on measured CH₄ for the midpoint month of each season using the California-specific emission model. The resulting χ^2 values were between 0.7–1.4 for most of the months except for November ($\chi^2 = 2.0$ with fit slope = 0.98 ± 0.05). Summer months showed

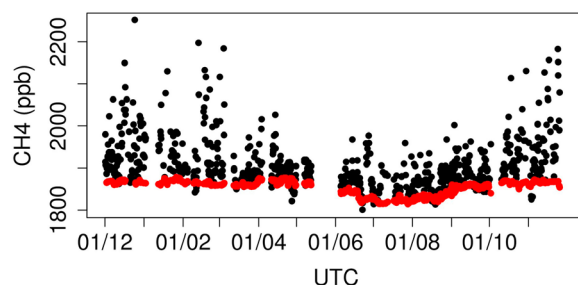


Figure 7. Time series (dates given as day/month) of measured CH₄ signals (black) and predicted background (red) CH₄ signals at 91 m on the WGC tower for well-mixed periods between 1 December 2007 and 30 November 2008.

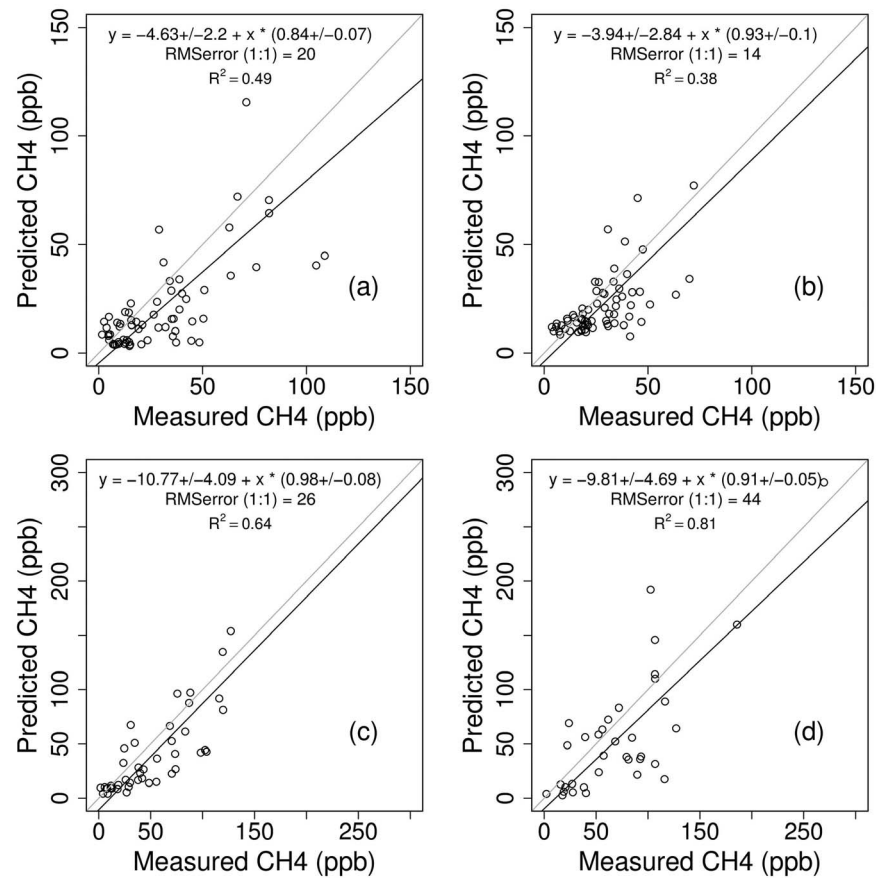


Figure 8. Comparison of CH₄ mixing ratios between measurements and predictions based on the final inverse optimization using California-specific emissions for the midpoint month of (a) spring, (b) summer, (c) fall, and (d) winter. For summer, June and July mixing ratios are compared together due to data removal during fire periods.

slightly lower-fitting slopes compared to the other months due to the large model-data mismatch error. Compared with the first inversion results, the seasonal slopes obtained from the final inversion are also closer to unity, and the reduced RMS errors are 19, 14, 25, and 43 ppb for spring, summer, fall, and winter, respectively. This result demonstrates that the two-step optimization procedure has improved the agreement between the measured and predicted CH₄ signals. Comparing the posterior scaling factors between the first and final inversions (Table 3), the two results are statistically consistent, suggesting that there are few significant differences for individual regions and seasons.

[32] From Table 3, we computed annual average scaling factors of 2.24 ± 0.26 , 1.57 ± 0.46 , and 1.17 ± 0.38 for

Regions 6, 7 and 8, respectively, using the final inversion results. This suggests that CH₄ emissions from Region 6 to the north of WGC (the southern end of the Sacramento Valley) are significantly higher than the California-specific model in the annual average. The seasonal variation in scaling factor for Region 6 decreases slightly in summer compared to spring and fall, partially diminishing the effect of increased summer time emissions present in the a priori model for rice agriculture. The scaling factors for Region 7 (Bay Area and surrounding urban areas) are also higher than the California-specific a priori model but show small increase in emissions in summer, in partial opposition to the change in Region 6. Scaling factors for Region 8 to the south of WGC (in the Northern San Joaquin Valley) appear

Table 3. Comparison of Posterior Scaling Factors Between First and Final (Second) Inversions for Each Season Based on the California-Specific Emission Model

Region	Spring		Summer		Fall		Winter	
	First	Final	First	Final	First	Final	First	Final
R06	2.61 ± 0.25	2.52 ± 0.27	2.25 ± 0.19	2.18 ± 0.24	2.56 ± 0.20	2.58 ± 0.24	1.83 ± 0.29	1.69 ± 0.31
R07	2.20 ± 0.45	1.60 ± 0.46	2.48 ± 0.42	1.91 ± 0.44	2.52 ± 0.45	1.53 ± 0.47	1.76 ± 0.48	1.23 ± 0.49
R08	1.05 ± 0.39	1.09 ± 0.40	1.07 ± 0.50	1.05 ± 0.50	0.84 ± 0.33	1.04 ± 0.37	1.63 ± 0.26	1.49 ± 0.27

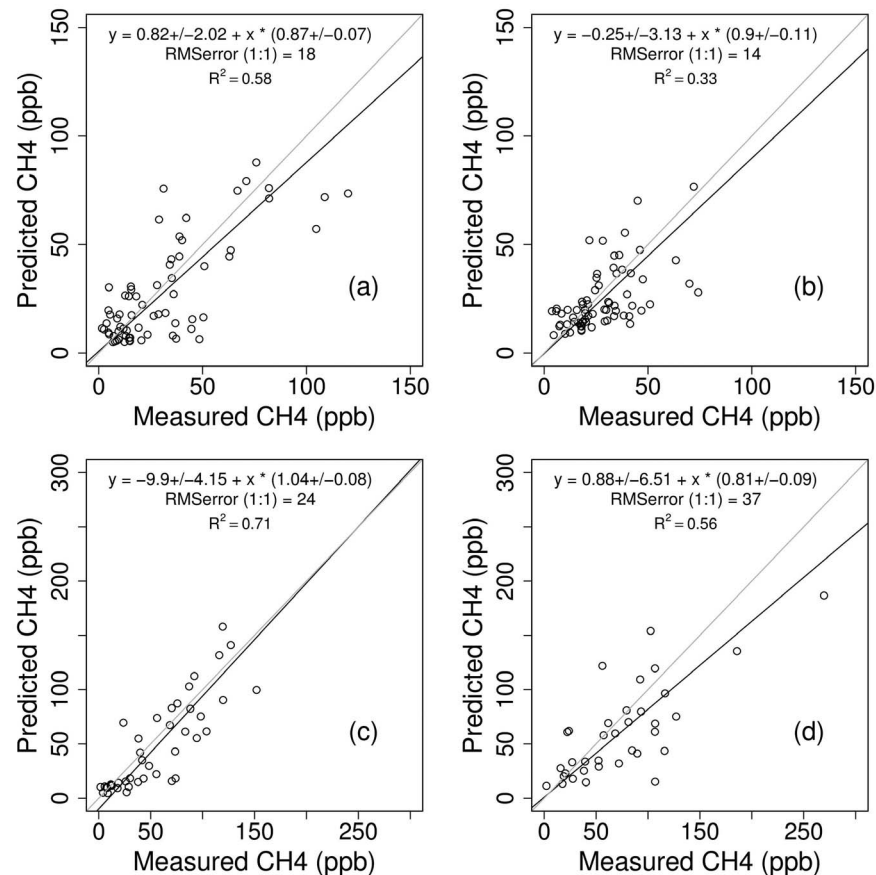


Figure 9. Comparison of CH₄ mixing ratios between measurements and predictions based on the final inverse optimization using EDGAR32 emissions for the midpoint month of (a) spring, (b) summer, (c) fall, and (d) winter. For summer, June and July mixing ratios are compared together due to data removal during fire periods.

approximately consistent with the California-specific model and show little seasonal variation, though there is a modest increase in winter.

[33] Following the above procedure, we performed similar analyses using EDGAR emission maps. First, we calculated predicted CH₄ signals using two different EDGAR emission models: EDGAR32 and EDGAR42 (EDGAR version 4.2) (European Commission Joint Research Centre (JRC) and Netherlands Environmental Assessment Agency, Emission Database for Global Atmospheric Research (EDGAR), release version 4.2, 2011, <http://edgar.jrc.ec.europa.eu>). Compared to EDGAR32, EDGAR42 provides emission maps at a much higher resolution ($0.1^\circ \times 0.1^\circ$) than EDGAR32, but the same resolution as that of the California-specific model. The fitting slopes based on EDGAR42 (0.44–0.57) were consistently lower than those of EDGAR32 (0.57–0.64) for all seasons. The RMS errors for EDGAR42 (30–77 ppb) were also higher than those of EDGAR32 (25–72 ppb) for all seasons. This result is due to the fact that the emission sum for Regions 6, 7 and 8 from the EDGAR42 emission maps is lower than that of EDGAR32 by a factor of 0.77. Compared to EDGAR32, EDGAR42 shows little change in the spatial distribution of CH₄ emissions and yields emission sums of 2.62, 5.73, and 3.16 Tg CO₂eq yr^{−1} for

Regions 6, 7 and 8, respectively. Compared to the California-specific model, the emission sum for Region 7 from EDGAR42 is still significantly higher by a factor of 4.48 while the emission sum for Region 8 is lower by a factor of 0.61 (see Table 1). Therefore, in this study we proceed with Bayesian inverse analyses only using EDGAR32 although our future study may reveal more information of the spatial distribution of CH₄ emissions using a priori emission models at different spatial scales and distributions.

[34] Figure 9 shows the comparison of posterior predicted and measured CH₄ signals from the final inversion (543 observations) using the EDGAR32 emission model for the midpoint month of each season. The resulting slopes and RMS errors are comparable to the inverse results with the California-specific model. This result suggests that the EDGAR32 model, used in combination with the measurements from this single tower, provides an equally good description of CH₄ emissions, despite the fact that the spatial resolution (~ 100 km) is much coarser than that of the California-specific emission map (~ 10 km). This result also suggests that a combination of the footprints spatial structure and errors in transport and background data do not allow us to distinguish emission estimates from the high-resolution emission maps from those of the low-resolution maps when

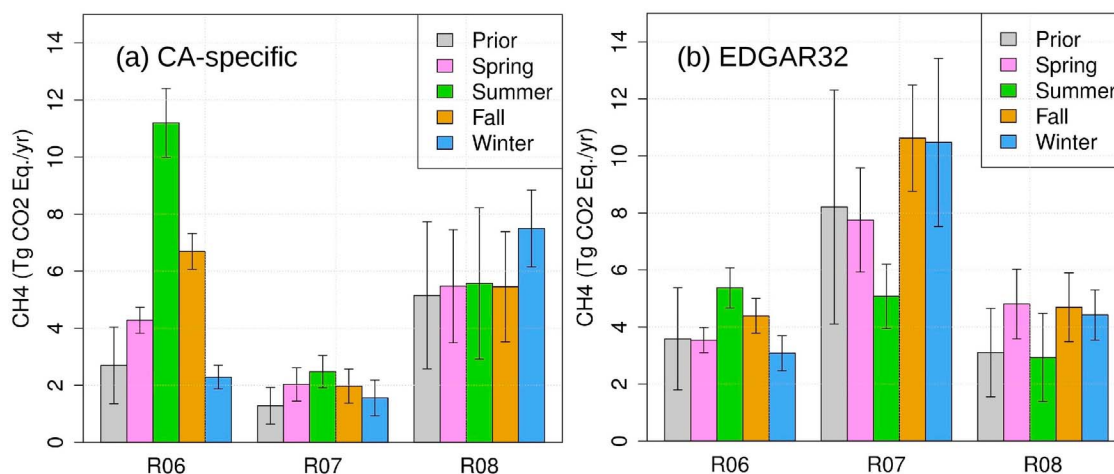


Figure 10. Comparison of posterior CH₄ emissions (Tg CO₂eq yr^{−1}, assuming a 100 year global warming potential of 21) by region between the (a) California-specific and (b) EDGAR32 emission models.

the emission model with a higher spatial resolution does not influence the inversion result significantly.

[35] Inferred CH₄ emissions are reported by region and as a regional sum over the region (6, 7, and 8) near the tower in Figure 10. Emission sums for the region from the California-specific emission model based on the 50% uncertainty assumption in the prior are 11.78 ± 2.11 , 19.25 ± 2.97 , 14.12 ± 2.12 , and 11.33 ± 1.54 Tg CO₂eq yr^{−1} (assuming a GWP of 21 g CO₂eq/g CH₄) for spring, summer, fall, and winter, respectively. However, the EDGAR32 model shows different seasonal emission sums for the region: 16.10 ± 2.24 , 13.38 ± 2.04 , 19.71 ± 2.30 , and 17.98 ± 3.13 Tg CO₂eq yr^{−1}. In particular, the emission sum for winter shows the largest difference. It appears that this discrepancy during winter is due to the difference in the emission distribution between the two prior models. The EDGAR32 model estimates more emissions in Region 7 while the California-specific model shows more emissions in Region 8 during winter. In Region 6, the EDGAR32 model shows seasonal variation with posterior scaling factors of 0.99 ± 0.12 , 1.50 ± 0.20 , 1.23 ± 0.17 , and 0.86 ± 0.17 for spring, summer, fall, and winter, respectively, but its seasonal variation is much smaller than that of the California-specific model, which has seasonal components driven by wetland and rice agriculture emissions. For Region 7, the EDGAR32 model shows the opposite seasonal variation to that of the California-specific model. The inversion based on the EDGAR32 model yields posterior scaling factors of 0.94 ± 0.22 , 0.62 ± 0.14 , 1.29 ± 0.23 , and 1.28 ± 0.36 for spring, summer, fall, and winter, respectively. Combined with the large emission sum for Region 7 from EDGAR32, which is ~6 times that of the California-specific model, seasonal variation in CH₄ emissions based on EDGAR32 is significantly different from that of the California-specific case. This difference between the two models will be discussed more in terms of correlations between regions. For Region 8, seasonal variation from the EDGAR32 model is small as was the case with the California-specific model.

[36] We then investigated the degree to which the tower footprints allow spatial resolution of emissions between the

different subregions by considering the off-diagonal elements of the posterior error covariance matrices and a priori emission model. In this regard, as Tarantola [1987] suggested, we derive correlations from the posterior covariance rather than a direct examination of the off-diagonal elements of the covariance. The correlations, which vary each month due to changing footprints, were generally negative between Regions 6 and 7 for both California-specific (−0.1 to −0.4) and EDGAR models (−0.2 to −0.8). The correlations between Regions 6 and 8 were also negative for both California-specific (−0.1 to −0.6) and EDGAR32 (−0.1 to −0.5) cases. It is worth noting that for the EDGAR32 case the anticorrelation is much stronger in Regions 6 and 7 than in Regions 6 and 8. It appears that this stronger anticorrelation in Regions 6 and 7 occurs when the EDGAR emission sum for Region 7, which is 2.7 times that of Region 8, is adjusted against Region 6 via the inversion system. This suggests that roughly 10–40% of emissions attributed to Region 6 in the California-specific emission model could be traded off against emissions from Region 7 and vice versa. This result further suggests that our inversion system has not solved the scaling factors entirely in an independent manner and only some linear combination of those scaling factors may be resolved.

3.4. Sensitivity Analysis

[37] A sensitivity analysis of prior uncertainty was conducted to investigate its impact on CH₄ emission estimates. With the 50% prior uncertainty as the baseline, we performed inversions using 70% and 90% prior uncertainties in the a priori emission models. The results showed that there is no significant change in CH₄ region sum estimates with different uncertainties in either the California-specific or EDGAR model. For the California-specific case, the region sums based on the 90% uncertainty case were 12.94 ± 3.18 , 20.97 ± 4.95 , 14.94 ± 3.05 , and 13.70 ± 2.24 Tg CO₂eq yr^{−1} for spring, summer, fall, and winter, respectively, which are not significantly different from the 50% uncertainty case: 11.78 ± 2.11 , 19.25 ± 2.97 , 14.12 ± 2.12 , and 11.33 ± 1.54 Tg CO₂eq yr^{−1}. Emissions from 70% uncertainty ranged

between these two results, showing no significant change in CH₄ emission estimates. The EDGAR-based inversion also showed no significant difference in the region sum for each season among different prior uncertainty assumptions.

[38] In addition to the prior uncertainty sensitivity analysis, we performed a sensitivity analysis on the observation period using observational data during the afternoon hours (12:00–17:00 local) as a subset of the original data. In this inversion, the number of 3 hourly observations is 284 while the number of unknowns is 130 as in the case of the original inversion. Based on the 50% uncertainty assumption in the a priori emission map, the final inversion using the California-specific emission model yielded emission sums of 12.12 ± 2.47 , 20.30 ± 3.12 , 17.55 ± 2.61 , and 12.83 ± 1.78 Tg CO₂eq yr⁻¹ for spring, summer, fall, and winter. Compared to those of the original inversion, we find that there is no significant difference between the two inverse analyses.

[39] We also conducted a sensitivity analysis on the α value used to remove outliers for the final inversion. We repeated the inversion using a fixed value of 2 for α instead of using varying values depending on the χ^2 statistic. In this inversion, the number of 3 hourly observations is 516, which is slightly smaller than 544 observations used in the original analysis. As *Bergamaschi et al.* [2005] indicated, the difference between the two analyses was small. The case based on the fixed value of 2 yields emissions sums of 11.12 ± 2.12 , 19.49 ± 2.96 , 14.84 ± 2.27 , 10.93 ± 1.73 Tg CO₂eq yr⁻¹ for spring, summer, fall, and winter, respectively, which are very similar to those of the case with varying α .

[40] Finally, 2008 included a period with significant fire activities and the data were initially screened to remove periods with obvious contamination from wild fires as described in section 2.1. We also investigated the sensitivity of emission estimates to the fire activities. When observations from the summer fire periods were not removed, the final inversion using the California-specific emission model yielded a region sum of 19.90 ± 2.96 Tg CO₂eq yr⁻¹ for Regions 6, 7 and 8 during the summer season, which does not deviate significantly from 19.25 ± 2.97 Tg CO₂eq yr⁻¹ of the original inversion. The inversion with the fire periods included showed 11.33 ± 1.20 , 2.65 ± 0.57 , and 5.92 ± 2.65 Tg CO₂eq yr⁻¹ for Regions 6, 7 and 8, respectively. This result is also comparable to 11.20 ± 1.21 , 2.48 ± 0.57 , and 5.57 ± 2.65 Tg CO₂eq yr⁻¹ from the original analysis.

4. Discussion

[41] The regionally summed annual posterior CH₄ emissions are 14.12 ± 2.19 and 16.79 ± 2.43 Tg CO₂eq for the California-specific and EDGAR32 models, larger than the sum of the California-specific prior (9.13 Tg CO₂eq) by factors of 1.55 ± 0.24 and 1.84 ± 0.27 , respectively. The similarity of these two factors suggests that inferred emissions for the area within approximately 150 km of the tower are independent of the two emission models and that actual summed CH₄ emissions are significantly higher than the sum inferred from the California ARB inventory. In terms of the spatial distribution of CH₄ emissions, these results indicate that the inversion system constrains emissions somewhat independent of the resolution of the emission map.

Assuming these average posterior scaling factors were applicable to all regions of California, the resulting total CH₄ emissions would comprise approximately 9% of total GHG emissions, a result that requires further investigation and confirmation (California ARB, online report, 2010).

[42] The California-specific a priori model shows clear seasonal variations in total CH₄ emissions, producing significantly greater total emissions in summer, moderate emissions in fall, and lower emissions in winter and spring. The higher summer time emissions are concentrated in Region 6, a result that is consistent with the spatial distribution and seasonality of the a priori emissions from rice agriculture [*Salas et al.*, 2006]. This provides consistent evidence for increased emissions in summer as expected in biological systems responding to warmer temperatures such as rice and wetlands [*Potter et al.*, 2006; *McMillan et al.*, 2007]. On the contrary, posterior emissions obtained with the EDGAR model yield only weak seasonality in total CH₄ emissions for the three regions although the fall and winter emissions are marginally different from those of the other seasons. In particular, the high winter emissions from the EDGAR model are likely due to a combination of urban emissions in the a priori model (i.e., ~six times larger than that of the California-specific model), its coarse spatial resolution, and weak footprints in the urban region during winter. It is conceivable that emissions from Region 7 might increase in winter due to urban emission sources such as increased natural gas use. However, it seems unlikely that natural gas emissions from Region 7 could drive the seven-fold increase in posterior emissions (10.47 ± 2.95 Tg CO₂eq yr⁻¹) compared to that (1.56 ± 0.62 Tg CO₂eq yr⁻¹) of the California-specific model, considering that natural gas accounts for only less than 30% of the total emission in Region 7. A further study is required to resolve this discrepancy, possibly using more measurements from multiple stations combined with additional improvements in a priori emission models.

[43] As described above, it appears that the different emissions models combined with the time varying footprints produce posterior emission sums that (1) peak in different regions and seasons and (2) contain anticorrelations among regions which limit unique spatial attribution of emissions. This type of anticorrelation in posterior emission estimates for different regions has been reported in the inversion results of *Bergamaschi et al.* [2005], and suggests that a network of measurement stations will be required to accurately resolve the spatial distributions of CH₄ emissions over the state of California [*Fischer et al.*, 2009].

[44] **Acknowledgments.** We thank Dave Field, Dave Bush, Edward Wahl, and particularly Jon Kofler for their assistance with the installation and maintenance of the instrumentation at WGC; Edward Dlugokencky for his advice and assistance in verifying the Picarro instrument performance at NOAA; John Lin, Steve Wofsy, Janusz Eluszkiewicz, and Thomas Nehrkorn for generously sharing the STILT code and providing advice; Chris Potter and William Salas for sharing modeled CH₄ emission for use as a priori estimates; Larry Hunsaker and Webster Tassat for providing the California ARB estimates of landfill CH₄ emissions; and Krishna Muriki for assistance in running WRF-STILT on the LBNL-Lawrencium computer cluster. We gratefully acknowledge NOAA Air Resources Laboratory (ARL) for the use of the HYSPLIT model underlying STILT and NCEP for the provision of the NARR meteorology. We also thank Jean Bogner, Eric Crosson, Guido Franco, Ying-Kuang Hsu, Eileen McCauley, and Tony VanCuren for valuable comments. This study was supported by the California Energy Commission (CEC) Public Interest Environmental Research Program and the Director, Office of Science, Office of Basic

Energy Sciences, U.S. Department of Energy under contract DE-AC02-05CH11231. The contribution of Chuanfeng Zhao for this work was partly performed under the auspices of the U.S. Department of Energy by the Lawrence Livermore National Laboratory under contract DE-AC52-07NA27344. The findings, views, and opinions presented in this paper do not necessarily represent the views and opinions of the California Energy Commission or the State of California.

References

- Alm, J., S. Saarnio, H. Nykänen, J. Silvola, and P. J. Martikainen (1999), Winter CO₂, CH₄, and N₂O fluxes on some natural and drained boreal peatlands, *Biogeochemistry*, **44**, 163–186, doi:10.1007/BF00992977.
- Ball, B. C., A. Scott, and J. P. Parker (1999), Field N₂O, CO₂ and CH₄ fluxes in relation to tillage, compaction and soil quality in Scotland, *Soil Tillage Res.*, **53**(1), 29–39, doi:10.1016/S0167-1987(99)00074-4.
- Bergamaschi, P., M. Krol, F. Dentener, A. Vermeulen, F. Meinhardt, R. Graul, M. Ramonet, W. Peters, and E. J. Dlugokencky (2005), Inverse modelling of national and European CH₄ emissions using the atmospheric zoom model TM5, *Atmos. Chem. Phys.*, **5**, 2431–2460, doi:10.5194/acp-5-2431-2005.
- Bianco, L., and J. M. Wilczak (2002), Convective boundary layer depth: Improved measurement by Doppler radar wind profiler using fuzzy logic methods, *J. Atmos. Oceanic Technol.*, **19**(11), 1745–1758, doi:10.1175/1520-0426(2002)019<1745:CBLDIM>2.0.CO;2.
- Bianco, L., J. M. Wilczak, and A. B. White (2008), Convective boundary layer depth estimation from wind profilers: Statistical comparison between an automated algorithm and expert estimations, *J. Atmos. Oceanic Technol.*, **25**, 1397–1413, doi:10.1175/2008JTECHA981.1.
- Bianco, L., I. V. Djalalova, C. W. King, and J. M. Wilczak (2011), Diurnal evolution and annual variability of boundary-layer height and its correlation to other meteorological variables in California's Central Valley, *Boundary Layer Meteorol.*, **140**, 491–511, doi:10.1007/s10546-011-9622-4.
- California Department of Conservation (2009), 2008 annual report of the state oil and gas supervisor, *Publ. PR06*, Sacramento, Calif. [Available at http://www.conservacion.ca.gov/dog/pubs_stats/annual_reports/Pages/annual_reports.aspx.]
- Cao, M., K. Gregson, and S. Marshall (1998), Global methane emission from wetlands and its sensitivity to climate change, *Atmos. Environ.*, **32**(19), 3293–3299, doi:10.1016/S1352-2310(98)00105-8.
- Christensen, T. R., I. C. Prentice, J. Kaplan, A. Haxeltine, and S. Sitch (1996), Methane flux from northern wetlands and tundra: An ecosystem source modeling approach, *Tellus, Ser. B*, **48**(5), 652–661, doi:10.1034/j.1600-0889.1996.t01-4-00004.x.
- Cicerone, R. J., J. D. Shetter, and C. C. Delwiche (1983), Seasonal variation of methane flux from a California rice paddy, *J. Geophys. Res.*, **88**, 11,022–11,024, doi:10.1029/JC088iC15p11022.
- Committee on Methods for Estimating Greenhouse Gas Emissions (2010), *Verifying Greenhouse Gas Emissions: Methods to Support International Climate Agreements*, 124 pp., Natl. Acad. Press, Washington, D. C.
- Dye, T. S., C. G. Lindsey, and J. A. Anderson (1995), Estimates of mixing depth from boundary layer radar profilers, paper presented at the 9th Symposium on Meteorological Observations and Instrumentation, Am. Meteorol. Soc., Charlotte, N. C.
- Fischer, M. L., C. Zhao, W. J. Riley, and A. C. Andrews (2009), Observation of methane and other non-carbon dioxide greenhouse gas emissions from California, *Rep. CEC-500-2009-096*, Public Interest Energy Res. Program, Calif. Energy Comm., Sacramento, Calif.
- Gerbig, C., J. Lin, S. Wofsy, B. Daube, A. E. Andrews, B. Stephens, P. S. Bakwin, and C. Grainger (2003), Toward constraining regional-scale fluxes of CO₂ with atmospheric observations over a continent: 2. Analysis of COBRA data using a receptor-oriented framework, *J. Geophys. Res.*, **108**(D24), 4757, doi:10.1029/2003JD003770.
- Gimson, N. R., and M. Uliasz (2003), The determination of agricultural methane emissions in New Zealand using receptor-oriented modelling techniques, *Atmos. Environ.*, **37**, 3903–3912, doi:10.1016/S1352-2310(03)00504-1.
- Göckede, M., A. M. Michalak, D. Vickers, D. P. Turner, and B. E. Law (2010), Atmospheric inverse modeling to constrain regional-scale CO₂ budgets at high spatial and temporal resolution, *J. Geophys. Res.*, **115**, D15113, doi:10.1029/2009JD012257.
- Hansen, S., J. E. Maehlum, and L. R. Bakken (1993), N₂O and CH₄ fluxes in soil influenced by fertilization and tractor traffic, *Soil Biol. Biochem.*, **25**(5), 621–630, doi:10.1016/0038-0717(93)90202-M.
- Harrison, M. R., T. M. Shires, J. K. Wessels, and R. M. Cowgill (1997), Methane emissions from the natural gas industry: Project summary, *Rep. EPA/600/SR-96/080*, U.S. Environ. Prot. Agency, Research Triangle Park, N. C.
- Hein, R., P. J. Crutzen, and M. Heimann (1997), An inverse modeling approach to investigate the global atmospheric methane cycle, *Global Biogeochem. Cycles*, **11**(1), 43–76, doi:10.1029/96GB03043.
- Hofmann, D. J., J. H. Butler, E. J. Dlugokencky, J. W. Elkins, K. Masarie, S. A. Montzka, and P. Tans (2006), The role of carbon dioxide in climate forcing from 1979 to 2004: Introduction of the Annual Greenhouse Gas Index, *Tellus, Ser. B*, **58**, 614–619, doi:10.1111/j.1600-0889.2006.00201.x.
- Houweling, S., T. Kaminski, F. Dentener, J. Lelieveld, and M. Heimann (1999), Inverse modeling of methane sources and sinks using the adjoint of a global transport model, *J. Geophys. Res.*, **104**(D21), 26,137–26,160, doi:10.1029/1999JD900428.
- Huang, Y., R. L. Sass, and F. M. Fisher (1998), A semi-empirical model of methane emission from flooded rice paddy soils, *Global Change Biol.*, **4**, 247–268, doi:10.1046/j.1365-2486.1998.00129.x.
- Intergovernmental Panel on Climate Change (1995), Climate change: IPCC second assessment report, Geneva, Switzerland.
- Janjić, Z. I. (1990), The step-mountain coordinate: Physical package, *Mon. Weather Rev.*, **118**, 1429–1443, doi:10.1175/1520-0493(1990)118<1429:TSMCPP>2.0.CO;2.
- Kort, E. A., J. Eluszkiewicz, B. B. Stephens, J. B. Miller, C. Gerbig, T. Nehrkorn, B. C. Daube, J. O. Kaplan, S. Houweling, and S. C. Wofsy (2008), Emissions of CH₄ and N₂O over the United States and Canada based on a receptor-oriented modeling framework and COBRA-NA atmospheric observations, *Geophys. Res. Lett.*, **35**, L18808, doi:10.1029/2008GL034031.
- Levin, I., et al. (2002), Three years of trace gas observations over the Euro-Siberian domain derived from aircraft sampling—A concerted action, *Tellus, Ser. B*, **54**, 696–712, doi:10.1034/j.1600-0889.2002.01352.x.
- Lin, J. C., C. Gerbig, S. C. Wofsy, A. E. Andrews, B. C. Daube, K. J. Davis, and C. A. Grainger (2003), A near-field tool for simulating the upstream influence of atmospheric observations: The Stochastic Time-Inverted Lagrangian Transport (STILT) model, *J. Geophys. Res.*, **108**(D16), 4493, doi:10.1029/2002JD003161.
- Lin, J. C., C. Gerbig, S. C. Wofsy, A. E. Andrews, B. C. Daube, C. A. Brainger, B. B. Stephens, P. S. Bakwin, and D. Y. Hollinger (2004), Measuring fluxes of trace gases at regional scales by Lagrangian observations: Application to the CO₂ Budget and Rectification Airborne (COBRA) study, *J. Geophys. Res.*, **109**, D15304, doi:10.1029/2004JD004754.
- Manning, A. J., D. B. Ryall, R. G. Derwent, P. G. Simmonds, and S. O'Doherty (2003), Estimating European emissions of ozone-depleting and greenhouse gases using observations and a modeling back-attribution technique, *J. Geophys. Res.*, **108**(D14), 4405, doi:10.1029/2002JD002312.
- Matsueda, H., and H. Y. Inoue (1999), Aircraft measurements of trace gases between Japan and Singapore in October of 1993, 1996, and 1997, *Geophys. Res. Lett.*, **26**(16), 2413–2416, doi:10.1029/1999GL900089.
- Matthews, R. B., R. Wassmann, and J. Arah (2000), Using a crop/soil simulation model and GIS techniques to assess methane emissions from rice fields in Asia. I. Model development, *Nutr. Cycling Agroecosyst.*, **58**, 141–159, doi:10.1023/A:1009894619446.
- McMillan, A. M. S., M. L. Goulden, and S. C. Tyler (2007), Stoichiometry of CH₄ and CO₂ flux in a California rice paddy, *J. Geophys. Res.*, **112**, G01008, doi:10.1029/2006JG000198.
- Mellor, G. L., and T. Yamada (1982), Development of a turbulence closure model for geophysical fluid problems, *Rev. Geophys.*, **20**, 851–875, doi:10.1029/RG020i004p00851.
- Mesinger, F., et al. (2006), North American Regional Reanalysis, *Bull. Am. Meteorol. Soc.*, **87**(3), 343–360, doi:10.1175/BAMS-87-3-343.
- Miller, S. M., et al. (2008), Sources of carbon monoxide and formaldehyde in North America determined from high-resolution atmospheric data, *Atmos. Chem. Phys.*, **8**, 7673–7696, doi:10.5194/acp-8-7673-2008.
- Montzka, S. A., E. J. Dlugokencky, and J. H. Butler (2011), Non-CO₂ greenhouse gases and climate change, *Nature*, **476**, 43–50, doi:10.1038/nature10322.
- Mosier, A., D. Schimel, D. Valentine, K. Bronson, and W. Parton (1991), Methane and nitrous oxide fluxes in native, fertilized and cultivated grasslands, *Nature*, **350**, 330–332, doi:10.1038/350330a0.
- Nehrkorn, T., J. Eluszkiewicz, S. C. Wofsy, J. C. Lin, C. Gerbig, M. Longo, and S. Freitas (2010), Coupled weather research and forecasting—Stochastic time-inverted Lagrangian transport (WRF-STILT) model, *Meteorol. Atmos. Phys.*, **107**, 51–64, doi:10.1007/s00703-010-0068-x.
- Office of Emergency Services (2008), California wildfires, *Map FEMA-EM-3287-CA*, Calif. Dep. of For. and Fire Prot., Sacramento, Calif. [Available at http://www.fire.ca.gov/downloads/incidents/All_statewide_Fires_0622_081108_a.pdf.]
- Olivier, J. G. J., J. A. Van Aardenne, F. Dentener, L. Ganzeveld, and J. A. H. W. Peters (2005), Recent trends in global greenhouse gas emissions: Regional trends and spatial distribution of key sources, in *Non-CO₂*

- Greenhouse Gases (NCGG-4)*, edited by A. van Amstel, pp. 325–330, Millpress, Rotterdam, Netherlands.
- Popa, M. E., M. Gloor, A. C. Manning, A. Jordan, U. Schultz, F. Haensel, T. Seifert, and M. Heimann (2010), Measurements of greenhouse gases and related tracers at Bialystok tall tower station in Poland, *Atmos. Meas. Tech.*, **3**, 407–427, doi:10.5194/amt-3-407-2010.
- Potosnak, M. J., S. C. Wofsy, A. S. Denning, T. J. Conway, J. W. Munger, and D. H. Barnes (1999), Influence of biotic exchange and combustion sources on atmospheric concentrations in New England from observations at a forest flux tower, *J. Geophys. Res.*, **104**(D8), 9561–9569, doi:10.1029/1999JD900102.
- Potter, C. S. (1997), An ecosystem simulation model for methane production and emission from wetlands, *Global Biogeochem. Cycles*, **11**(4), 495–506, doi:10.1029/97GB02302.
- Potter, C., S. Klooster, S. Hiatt, M. Fladeland, V. Genovese, and P. Gross (2006), Methane emissions from natural wetlands in the United States: Satellite-derived estimation based on ecosystem carbon cycling, *Earth Interact.*, **10**, 1–12, doi:10.1175/EI200.1.
- Press, W. H., S. A. Teukolsky, W. T. Vetterling, and B. P. Flannery (1992), *Numerical Recipes in FORTRAN*, 2nd ed., Cambridge Univ. Press, Cambridge, U. K.
- Salas, W., P. Green, S. Frolking, C. Li, and S. Boles (2006), Estimating irrigation water use for California agriculture: 1950s to present, *Rep. CEC-500-2006-057*, Public Interest Energy Res. Program, Calif. Energy Comm., Sacramento, Calif.
- Salas, W., C. Li, F. Mitloehner, and J. Pisano (2009), Developing and applying process-based models for estimating greenhouse gas and air emissions from California dairies, *Rep. CEC-500-2008-093*, Public Interest Energy Res. Program, Calif. Energy Comm., Sacramento, Calif.
- Simpson, I. J., G. C. Edwards, G. W. Thurtell, G. den Hartog, H. H. Neumann, and R. M. Staebler (1997), Micrometeorological measurements of methane and nitrous oxide exchange above a boreal aspen forest, *J. Geophys. Res.*, **102**(D24), 29,331–29,341, doi:10.1029/97JD03181.
- Skamarock, W. C., J. B. Klemp, J. Dudhia, D. O. Gill, D. M. Barker, W. Wang, and J. G. Powers (2005), A description of the advanced research WRF version 2, *Tech. Note NCAR/TN-468+STR*, Natl. Cent. for Atmos. Res., Boulder, Colo.
- Tarantola, A. (1987), *Inverse Problem Theory Methods for Data Fitting and Model Parameter Estimation*, 613 pp., Elsevier, New York.
- Tian, H., X. Xu, M. Liu, W. Ren, C. Zhang, G. Chen, and C. Lu (2010), Spatial and temporal patterns of CH₄ and N₂O fluxes in terrestrial ecosystems of North America during 1979–2008: Application of a global biogeochemistry model, *Biogeosciences*, **7**(9), 2673–2694, doi:10.5194/bg-7-2673-2010.
- Werner, C., K. Davis, P. Bakwin, C. Yi, D. Hurst, and L. Lock (2003), Regional-scale measurements of CH₄ exchange from a tall tower over a mixed temperate/boreal lowland and wetland forest, *Global Change Biol.*, **9**, 1251–1261, doi:10.1046/j.1365-2486.2003.00670.x.
- Wilson, J. O., P. M. Crill, K. B. Bartlett, D. I. Sebach, R. C. Harriss, and R. L. Sass (1989), Seasonal variation of methane emissions from a temperature swamp, *Biogeochemistry*, **8**, 55–71, doi:10.1007/BF02180167.
- Wratt, D. S., N. R. Gimson, G. W. Brailsford, K. R. Lassey, A. M. Bromley, and M. J. Bell (2001), Estimating regional methane emissions from agriculture using aircraft measurements of concentration profiles, *Atmos. Environ.*, **35**, 497–508, doi:10.1016/S1352-2310(00)00336-8.
- Zhang, Y., C. Li, X. Zhou, and B. Moore (2002), A simulation model linking crop growth and soil biogeochemistry for sustainable agriculture, *Ecol. Modell.*, **151**, 75–108, doi:10.1016/S0304-3800(01)00527-0.
- Zhao, C., A. E. Andrews, L. Bianco, J. Eluszkiewicz, A. Hirsch, C. MacDonald, T. Nehrkorn, and M. L. Fischer (2009), Atmospheric inverse estimates of methane emissions from central California, *J. Geophys. Res.*, **114**, D16302, doi:10.1029/2008JD011671.